Kinetics and Mechanism of the Formation of Ag Nanoparticles by Electrochemical Techniques: A Plasmon and Cluster Time-Resolved Spectroscopic Study

M. Luisa Rodríguez-Sánchez,[†] M. José Rodríguez,[†] M. Carmen Blanco,[†] José Rivas,[‡] and M. Arturo López-Quintela*[,†]

Laboratory of Magnetism and Nanotechnologies, Institute of Technology, Departments of Physical Chemistry and Applied Physics, University of Santiago de Compostela, E-15782 Santiago de Compostela, Spain

Received: September 1, 2004; In Final Form: October 26, 2004

The formation of Ag nanoparticles by electrochemical techniques has been investigated through a time-resolved UV−vis spectroscopy study. The formation of Ag_4^{2+} clusters is suggested as the main precursors to the particle formation. The mechanism also considers the electrodeposition which occurs as a parallel process in the electrochemical particle formation. Experiments at different current densities show that the electrodeposition is more important at low current densities. From the fittings of the change of the plasmon ($\lambda \approx 430$ nm) and the cluster ($\lambda = 250$ nm) bands to the proposed mechanism, the kinetic constants of the formation and disappearance of the Ag_4^{2+} cluster are derived. The kinetic fittings also allowed an estimation of the Ag_4^{2+} cluster extinction coefficient ($\epsilon_{250} = 1.0 \times 10^4$ M^{-1} cm^{-1}). It is observed that the plasmon bandwidth (fwhm) follows the theoretical predicted $1/R$ law only for particles with sizes $d \gtrsim 3$ nm, but the law is broken for the smallest particles ($d < 2.5$ nm). The break is associated with the existence of single-electron (SE) transitions which are activated by the plasmon decay for the smallest nanoparticles. From the broken $1/R$ law, a limit relaxation time of about 4 fs is derived for the plasmon deactivation. Below this limit, the plasmon seems to decay mainly through a nonradiative channel with the formation of electron−hole (e−h) pairs. By comparison of the $1/R$ broken law with other literature results, it is concluded that large interactions of the Ag nanoparticles with the used capping molecule (tetrabutylammonium acetate) facilitate the e−h plasmon deactivation.

I. Introduction

The preparation of nanoparticles of controlled size is, nowadays, one of the most interesting topics in applied sciences because of the wide range of possible applications, which include, among others, new catalyzers,[1] surface-enhanced Raman spectroscopy (SERS),[2] ultrahigh-density magnetic storage,[3] biosensors,[4] and so forth. For this purpose it is very important to have simple and economical synthetic routes which can be applied in large scales as it is needed for most industrial applications. Among the soft chemical methods to produce nanoparticles, such as microemulsions,[5] organometallics,[6] surfactants, polymers,[7] and so forth, electrochemical techniques, first introduced by Reetz et al.[8] in 1994, are very promising because of their simplicity. By using galvanostatic conditions, a sacriphicial metal sheet as the metal ion source, and a trapping/capping molecule, these authors were able to prepare different metal particles. Two years later, Zoval et al.[9] observed the formation of silver nanoparticles on graphite surfaces using an aqueous solution of silver ions and a large overpotential during a short single plating pulse. This technique was further developed to produce metal oxide and semiconductor nanoparticles deposited on graphite by means of a hybrid electrochemical/chemical synthesis.[10] In parallel, the Reetz's technique was also further developed to produce other type of metals,[11] metal oxides,[12] and nonspherical particles.[13] Very recently Reetz et al.[14] have reviewed this technique including a systematic study of the influence of different parameters (such as solvent polarity, charge flow, temperature, solvent, etc.) on the final particle size distribution. However, the mechanism of formation of particles, synthesized by both techniques (a) galvanostatic with trapping and (b) constant voltage without trapping, remains to be clarified. In particular, it is not clear which is the role of the main parameters controlling the final particle size. Until now, mainly thermodynamic arguments have been employed to explain the dependence of the particle size on the current density for technique a,[8] whereas kinetic arguments, corresponding to a separate fast nucleation and a slow growth, have been employed to explain the size polydispersity in technique b.[9] Because the knowledge of the mechanisms involved in the formation of particles is very important for preparing monodisperse nanoparticle samples, we have carried out a time-resolved UV−vis spectrophotometric study of the kinetics of formation of Ag nanoparticles using galvanostatic conditions (technique a). It is observed that the formation of particles proceeds through the formation of specific Ag precursor clusters. A mechanism for the formation of particles through those clusters is proposed. Furthermore, the study of the plasmon band dependence on the particle size allowed us to derive some interesting conclusions about the damping of the surface plasmon resonance. The results can be explained assuming the existence of a nonradiative decay channel excited by the stabilizer protecting the particles. The obtained results can be

* To whom correspondence should be addressed. E-mail: qfarturo@usc.es.
[†] Department of Physical Chemistry.
[‡] Department of Applied Physics.

10.1021/jp046056n CCC: $30.25
Published on Web 12/30/2004

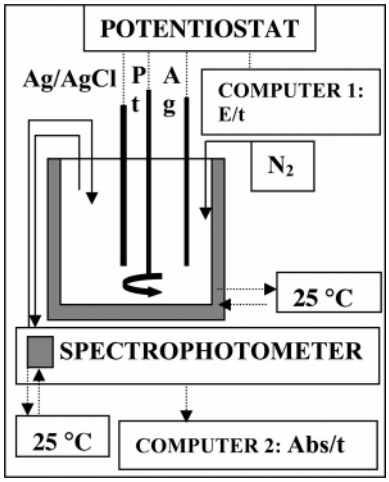

Figure 1. Scheme of the experimental device used for the synthesis and time-resolved spectroscopic study of the formation of Ag nanoparticles.

of interest in "hot" fields such as the design of plasmon−polariton modes which can be used for guiding electromagnetic energy below the diffraction limit.[15] The paper is organized as follows: after the Experimental Section, we will show the time-resolved spectral study in section III.1. Then, a possible mechanism is proposed in section III.2. Section III.3 is devoted to the study of the properties of the plasmon band. Discussion is given in section IV, and finally, the most important conclusions are displayed in section V.

II. Experimental Section

Nanoparticle Synthesis. All chemicals were of analytical grade and used without further purification: tetrabutylammonium acetate (TBAAcO) and acetonitrile from Aldrich; aluminum oxide, α, 99.99%, 1.0 μm from Alfa. An Autolab PGSTAT 20 potentiostat was used both in the synthesis and the electrochemical study. Temperature was kept at 25 ± 0.1 °C using a Grant thermostatic bath. All potentials were measured against an Ag/AgCl reference electrode. The syntheses were carried out in a standard Metrohm electrolysis beaker containing a sacrificial silver sheet as anode (counter electrode), and a platinum sheet of the same size as the silver sheet was used as cathode (working electrode). These two electrodes were vertically placed face-to-face at a constant distance of 0.5 cm. The platinum electrode was hand-polished with 1 μm alumina powder to a mirror like finish. Then, the electrode was activated by triangular potential cycling between 1.35 and −0.15 V, at a scan rate of 500 mV s^{-1} for 5 min in 1.0 M H_2SO_4. Before each experiment, the silver electrode was hand polished with a fine grade emery paper and washed with bidistillated water and a small amount of acetone. The electrolyte solution containing 0.1 M tetrabutylammonium acetate in acetonitrile was deaerated by bubbling nitrogen for about 15 min, keeping inert atmosphere during the whole process. A freshly prepared solution was used in each experiment. Strong stirring was kept during the galvanostatic electrolysis.

Time-Resolved Experiments. Figure 1 shows a scheme of the experimental device. As can be seen, computer 1 continuously records the potential against time measured from the potentiostat. Measurements of absorption spectra were taken also in a continuous manner. For this purpose, a peristaltic micropump was coupled to the system, pumping the solution to a 1 cm light path length Hellma cuvette of a diode-array Hewlett-Packard HP8452 spectrophotometer. Spectra were recorded every 30 s in the range 240−650 nm during the nanoparticle synthesis, and data were recorded in computer 2.

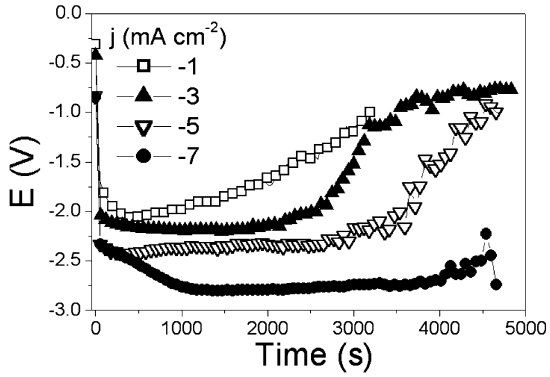

Figure 2. Change of the electrode potential during the nanoparticle synthesis at different current densities (*j*).

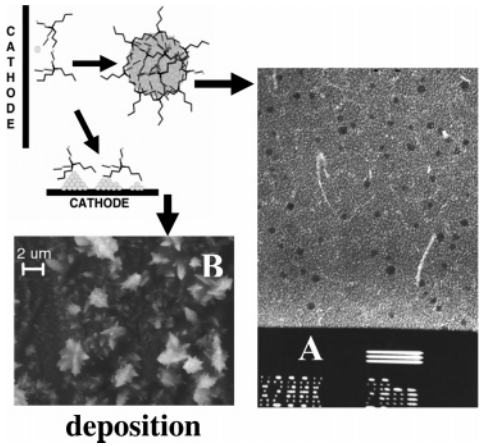

Figure 3. Schematic picture showing the competition of two processes: (A) silver nanoparticle formation; (B) silver deposition on Pt. The inserted microphotographs correspond to TEM (A) and SEM (B) pictures of both processes (particles and electrode surface).

Ag^+ Estimation. The Ag^+ concentration in the colloidal dispersions was estimated by a turbidimetric method.[16] At a particular time *t*, two samples were removed from the synthesis medium. The first sample was used to fix the 100% of transmittance. An excess of chloride was added to the second sample, and the transmittance was immediately measured. The measurements were recorded at 800 nm.

III. Results

III.1. Time-Resolved Experiments. *Potential Change.* In Figure 2, one can see the variation of the potential during the particle synthesis at different current densities. It is observed that the potential increases (becomes more negative) very fast attaining high overpotential values in the range 1.2−2.0V, depending on the employed current density. After that, the potential remains approximately constant, mainly at high current densities. In the final stages, the potential decreases approaching the equilibrium potential (−0.8 V). When this occurs, the formation of the particles stops. In a previous work,[11] we have seen that these changes in the potential are related to the existence of two competing processes, which are summarized in Figure 3. One of these processes corresponds to the formation of nanoparticles and the other to the deposition onto the electrode. When the Pt electrode is completely covered with Ag, the electrodeposition is more favorable than the formation of particles; the potential goes down to the equilibrium potential,

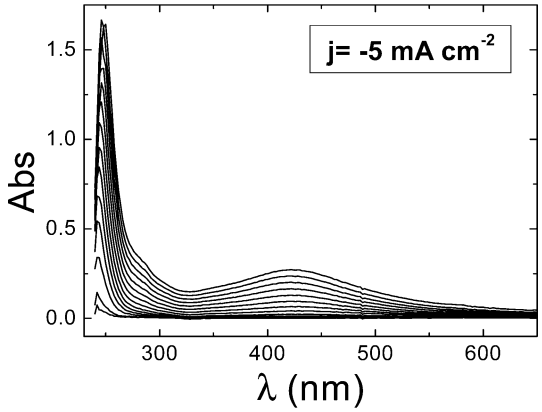

Figure 4. Absorbance versus time during the electrochemical synthesis of Ag nanoparticles carried out at $j = -5$ mA cm^{-2}. Time between successive spectra is $\Delta t = 30$ s.

and the particle formation stops. This is associated with a decrease in the potential (decrease of the Gibbs free energy). It was also observed[11] that the electrodeposition is more effective at low current densities, and therefore, the decrease of the potential associated with this process is observed at earlier times (see Figure 2). On the other hand, the observed initial increase of the potential can be associated with the increase of the [Ag^+], because at the beginning of the electrolysis [Ag^+] = 0, and only after a certain time (~500 s) it reaches a stationary state (ss).[17] When this occurs, the electrochemical potential remains approximately constant, as it is clearly observed in the curves shown in Figure 2. However, at the lowest current density, −1 mA cm^{-2}, a continuous and slow potential increase is observed already from the beginning, because of the relative increase in importance of the electrodeposition in the whole process, as it was previously established.[11]

As we have shown in a previous study,[11] the current density has a big influence not only on the electrodeposition process but also on the particle formation. In agreement with different studies about the formation of other kinds of particles, it is found that the average particle size diminishes by increasing the current density. This result has been interpreted assuming that the particle size is given by the critical nucleus size of the adatoms formed at the electrode surface,[8] which, in turn, depends on the overpotential. However, as we will see later on, this explanation is not completely correct, and other factors must be taken into account to explain this result.

UV−Vis Spectra Change. Figure 4 shows the change of the absorbance with time for a typical synthesis at $j = -5$ mA cm^{-2}. A very broad plasmon band is observed with a maximum located at ≈425−430 nm. The appearance of another two bands, located in the UV region at 242−254 and 280−284 nm depending on the experimental conditions, is also observed. These bands appear before the plasmon band arises, and this can be taken as an indication that some precursor species are formed before the formation of the final particles.

Band Identification. There have been a lot of studies done in the past about the identification of bands attributed to different Ag clusters. Although there are many aspects of the identification of the bands which still remain unclear, we have used the available information for a first tentative identification of the bands we have observed. Most of the works have been performed by Henglein et al.[18] and refer to clusters stabilized in water solutions. The main peak centered at around 250 nm, which is the first which appears in our experiments, could be identified with the cluster Ag_4^{2+}. In water solutions, this cluster shows a band at 265−275 nm.[19−22] The small blue shift

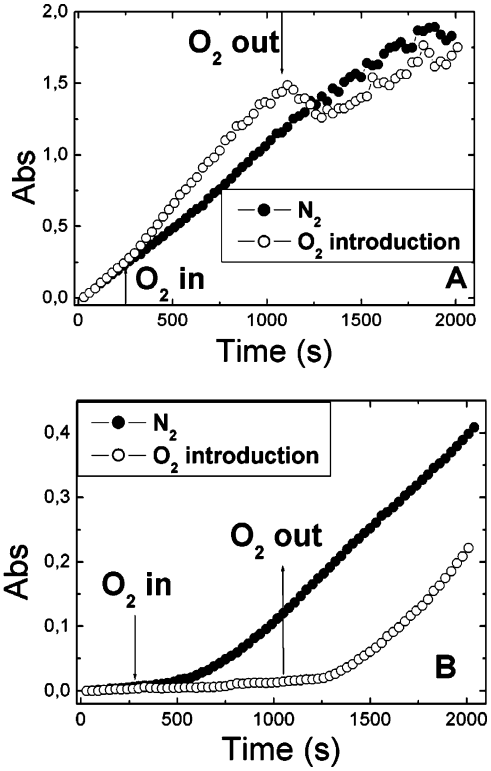

Figure 5. Absorbance variation during the synthesis of Ag nanoparticles at (A) 250 nm and (B) 428 nm in N_2 atmosphere and introducing O_2 ($j = -5$ mA cm^{-2}).

observed in our case could be explained because of the smaller polarity of the medium we use. The Ag_4^{2+} cluster is the most stable one among the observed Ag clusters and is the only one which is stable against oxidation.[23] To check this aspect and confirm that this band corresponds to the Ag_4^{2+} cluster, we have conducted experiments in which we externally introduced oxygen into the system. In Figure 5A, it is shown that after introduction of oxygen at a given time into the system the concentration of these clusters not only does not decrease but even increases (greater absorbance than in absence of oxygen). This may be attributed to the disappearance of the other less-stable clusters, as we will discuss later on. Cutting again the introduction of oxygen into the system, the absorbance recovers again showing values corresponding to the concentration in absence of oxygen. It can be also observed that, at the beginning of the electrolysis, both curves, in the presence and absence of oxygen, coincide. This would indicate that, at the beginning, this is the predominant cluster present in the system, and therefore, the reaction proceeds almost exclusively to the formation of this cluster. For comparison purposes, we show in Figure 5B the evolution of the plasmon band. It can be observed that there is an initial "induction" period during which no particles are formed. In a previous publication,[11] we attributed the existence of this "induction period" to an autocatalysis mechanism. However, we can clearly see now that there is no autocatalysis and that the presence of this "induction period" corresponds to the period in which the Ag precursor clusters are being formed. One can also see that this period increases very much when oxygen is present in the system, which is an indication that the formation of other intermediate clusters, different from Ag_4^{2+}, is more difficult in the presence of oxygen. In Figure 6 the evolution of the peak which we have attributed to the Ag_4^{2+} cluster (250 nm) is compared with the other one detected at 284 nm. It can be seen that the absorbance at 284

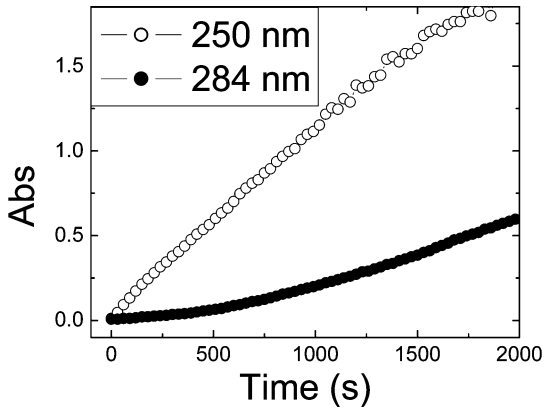

Figure 6. Absorbance versus time for the peaks centered at 250 and 284 nm corresponding to an electrolysis carried out at $j = -7$ mA cm^{-2}.

nm evolves more slowly than the Ag_4^{2+} peak and, therefore, can be attributed to another (larger) intermediate cluster, which could be ascribed to Ag_8^{+} according to the literature.[24] However, the absorbance band of this intermediate is small and in some cases almost undetected. We will therefore consider it as a short-lived intermediate ("in comparison with the most stable one"), and it will not be considered further for the kinetic study.

We finally mention that there is a recent high interest on Ag_n clusters showing fluorescence.[25−28] Until now, fluorescence in clusters with $1 \le n \le 8$ has been found. In our case, we have also observed a complicated fluorescence behavior (results not shown) which indicates the existence of, at least, two fluorescence species, which could be related with the two cluster species identified by the absorption studies.

III.2. Mechanism. According to the previous results, we propose the following mechanism for the formation of the Ag nanoparticles:

SCHEME 1

[1] $Ag^+ + e^- \xrightarrow{k_1} Ag^0$

[2] $Ag^0 + Ag^+ \xrightarrow{k_2} Ag_2^+$

[3] $2Ag_2^+ \xrightarrow{k_3} Ag_4^{2+}$

[4.1] $Ag_4^{2+} + 2e^- \xrightarrow{k_{4.1}} Ag_4^0$

[4.2] $Ag_4^0 + Ag^+ \xrightarrow{k_{4.2}} Ag_5^+$

[5.1] $Ag_5^+ + e^- \xrightarrow{k_{4.1}} Ag_5$

...

[$(n-1)$.1] $Ag_{n-1}^+ + e^- \xrightarrow{k_{4.1}} Ag_{n-1}$

[$(n-1)$.2] $Ag_{n-1} + Ag^+ \xrightarrow{k_{4.2}} Ag_n^+$

[n] $Ag_n^+ + e^- \xrightarrow{k_{4.1}} Ag_n$

Assuming a stationary state (ss) for the species Ag^0 and Ag_2^+, one can arrive at the following expression:

$$[Ag^0] = (k_1/k_2)\exp(-\alpha\phi_1) \qquad (1)$$

where α is the transfer coefficient and $\phi_1 = F\eta_1/RT$, F being the Faraday constant, R the gas constant, and T the absolute temperature. Then, one can write

$$\frac{d[Ag_4^{2+}]}{dt} = \frac{k_1}{2}\exp(-\alpha\phi_1)[Ag^+] - k_{4.1}\exp(-2\alpha\phi_2)[Ag_4^{2+}] \qquad (2)$$

where we have assumed that the transfer coefficients are the same for both species.

We have seen that (section III.1), after an initial period of time, $[Ag^+]$ seems to attain a constant ss value, $[Ag^+]_{ss}$. Then, considering that $[Ag_4^{2+}] = A_{250}/\epsilon_{250}$ (A_{250} and ϵ_{250} being the absorbance and extinction coefficient at $\lambda = 250$ nm, respectively), one obtains

$$\frac{dA_{250}}{dt} = b_1 - b_2A_{250} \qquad (3)$$

where $b_1 = \epsilon_{250}(k_1/2)\exp(-\alpha\phi_1)[Ag^+]_{ss}$ and $b_2 = k_{4.1}\exp(-2\alpha\phi_2)$. In Figure 7, it is plotted $\ln(b_1 - b_2A_{250})$ against time for the electrolysis performed at -8 mA cm^{-2}. It is shown that the data agree with eq 3. The values of the parameters obtained after an iterative fitting are $b_1 = (4.0 \pm 1) \times 10^{-3}$ s^{-1} and $b_2 = (5 \pm 3) \times 10^{-4}$ s^{-1}. However, the fitting becomes poorer at large times, and this is more important at low current densities as it can be seen in Figure 8 corresponding to the synthesis carried out at $j = -1$ mA cm^{-2}. It is interesting to notice that, from the fitting of the first part of the curve shown in Figure 8, the same values of the parameters are obtained indicating that the rate constant remains approximately unchanged with the current density.

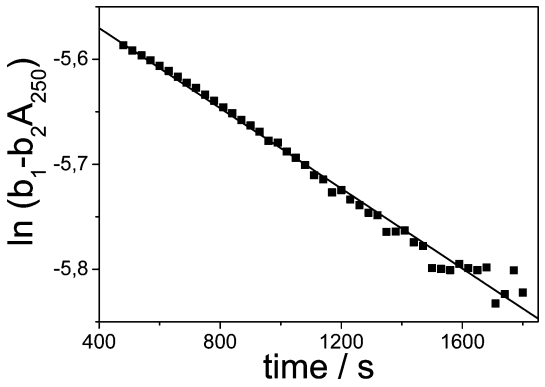

Figure 7. Plot of $\ln(b_1 - b_2A_{250})$ vs time for an electrolysis performed at $j = -8$ mA cm^{-2}.

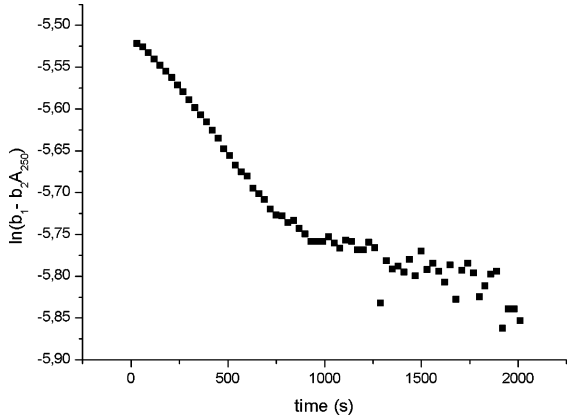

Figure 8. Plot of $\ln(b_1 - b_2A_{250})$ vs time for an electrolysis performed at $j = -1$ mA cm^{-2}.

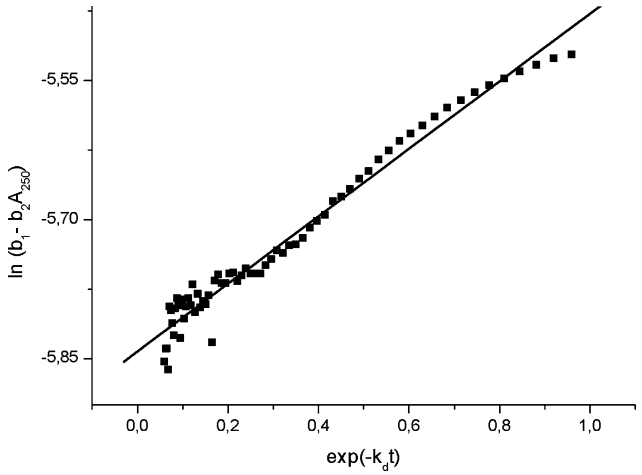

Figure 9. Representation of $\ln(b_1 - b_2A_{250})$ vs $\exp(-k_dt)$ for the data shown in Figure 8 corresponding to an electrolysis carried out at $j = -1$ mA cm^{-2}.

The deviation of the fittings, mostly observed at low current densities, is due to the fact that another competing process, namely, the electrodeposition, which is important at longer times, has not been taken into account. To account for this process, one can introduce the effective area of the electrode, S, in eq 2. Assuming further that this effective area decreases exponentially with time ($S = S_0 \exp(-k_dt)$), the following equation can be obtained:

$$\ln(b_1 - b_2A_{250}) = \left[\ln b_1 + \frac{S_0b_2}{k_d}\right] + \frac{S_0b_2}{k_d}\exp(-k_dt) \quad (4)$$

Figure 9 shows the representation of eq 4 considering the previous values obtained for the parameters b_1 and b_2. Although the fitting is not very good at short times, as a result of the simplified assumption of the exponential decrease of the electrode surface with time, the value obtained for the fitted parameter, k_d, was in the range $(1.4-3.4) \times 10^{-3}$ s^{-1}, which is very reasonable (see below). From this fitting, one can obtain the value of the initial electrode surface, $S_0 = 2.0$ cm^2. This value is similar to the experimental value used ($S_0 = 2.5$ cm^2).

For the later steps of the mechanism which follow the formation of the Ag_4^{2+} cluster, one can make the following simplification: taking into account the big stability of the Ag_4^{2+} cluster and to get information about the steps which follow the formation of this small cluster, we can assume that the slowest of the steps (reactions 4.1$-n$) is the decomposition of the Ag_4^{2+} cluster because of its large stability. Then we can write

$$\frac{d[Ag]_P}{dt} = \frac{\sum_{i=4} d[Ag_n]}{dt} = k_{4.1}[Ag_4^{2+}]\exp(-2\alpha\phi_2) = b_2[Ag_4^{2+}] \quad (5)$$

The concentration of the particles can be related to the plasmon band ($A_P = \epsilon_P[Ag]_P$, where A_P is the absorbance at the maximum of the plasmon band and ϵ_P is the extinction coefficient at the maximum). Then we can write

$$\frac{dA_P}{dt} = b_2\left(\frac{\epsilon_P}{\epsilon_{250}}\right)A_{250} \quad (6)$$

which relates the evolution of the plasmon and the Ag_4^{2+} cluster bands.

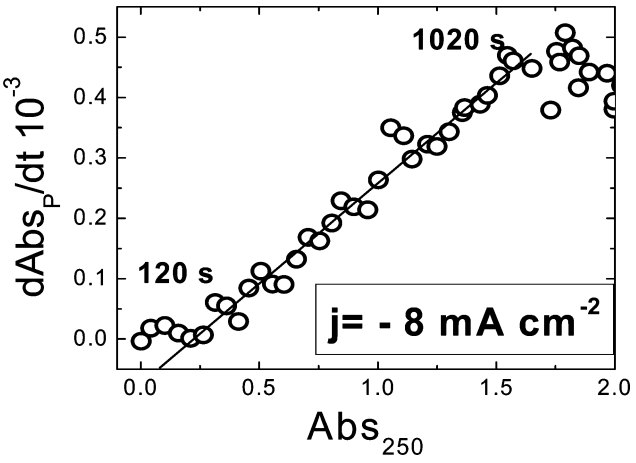

Figure 10. dA_P/dt versus A_{250} for an electrolysis carried out at $j = -8$ mA cm^{-2}.

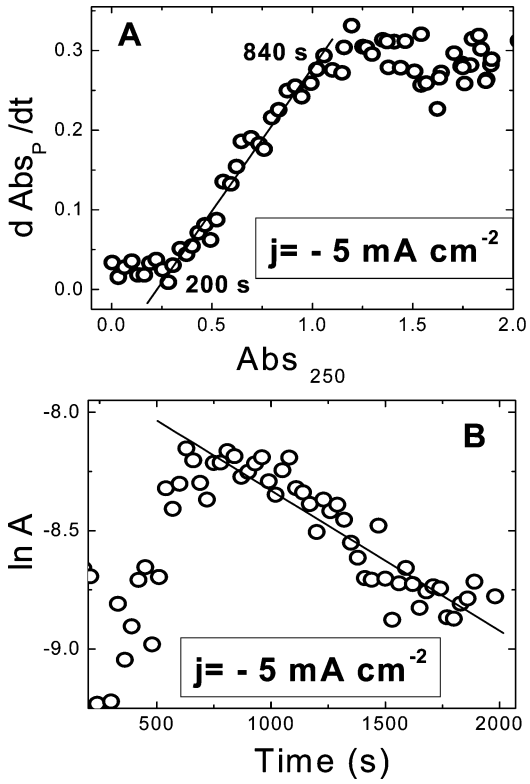

Figure 11. Representation of eqs 6 (A) and 7 (B) showing the effect of the electrodeposition on the Ag nanoparticle formation.

In Figure 10, it can be observed that eq 6 adequately interprets the data. From the fitting, a value of $\epsilon_P/\epsilon_{250} = 0.7$ can be derived. It has to be said that again the fitting becomes poorer at large times and that this deviation is more important at low current densities because in eq 6 we have not considered the electrodeposition. If one considers the simultaneous electrodeposition, introducing the same assumptions as before, one can obtain from eq 6 the following equation:

$$\ln\left[\frac{\left(\frac{dA_P}{dt}\right)}{A_{250}}\right] = \ln\left[b_2\left(\frac{\epsilon_P}{\epsilon_{250}}\right)\right] - k_dt \quad (7)$$

In Figure 11, both fittings (eqs 6 and 7) are shown for an intermediate current density. It can be clearly seen that eq 6 adequately describes the data at short times, but at large times, one has to take the electrodeposition into account for the

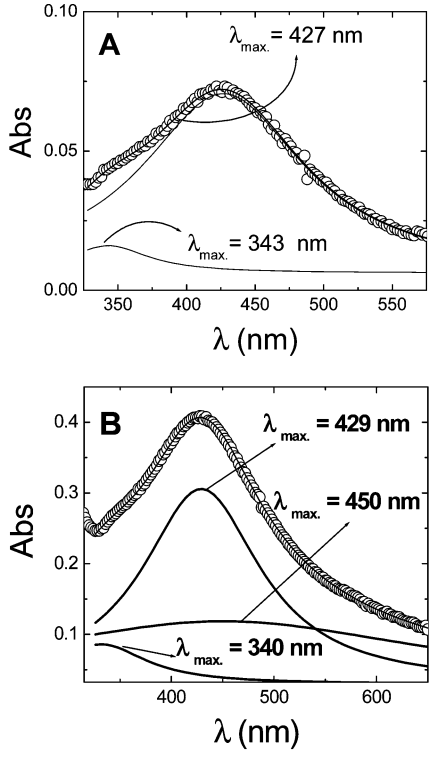

Figure 12. Plasmon band and their corresponding fittings at two different times, $t = 810$ s (A) and $t = 1980$ s (B), for an electrolysis carried out at $j = -5$ mA cm^{-2}.

TABLE 1: Deposition Rate Constant, k_d, Obtained from Eq 7 at Different Current Densities

j (mA cm^{-2})	k_d (s^{-1})
−1	$(1.3 \pm 0.1) \times 10^{-3}$
−3	$(1.2 \pm 0.1) \times 10^{-3}$
−5	$(6.0 \pm 0.1) \times 10^{-4}$
−7	$(5.1 \pm 0.1) \times 10^{-4}$
−8	$(5.7 \pm 0.7) \times 10^{-4}$

interpretation of the data. In any case, the kinetic parameters obtained from the different fittings are very similar. The final mean values of the kinetic constants which can be obtained are $b_1 = 2.2 \times 10^{-3}$ s^{-1} and $b_2 = 9.3 \times 10^{-4}$ s^{-1}. It is interesting to note that the obtained kinetic constants do not change with the current density. However, in agreement with what has been observed before,[11] the deposition rate constant obtained from the fittings decreases as the current density increases, as can be seen in Table 1. From a Tafel plot, a value of $\alpha\phi_2 = -2.2$ was obtained. Then, from the b_2 values obtained from the fittings, one can finally obtain the rate constant for the assumed slowest step of the mechanism, $k_{4.1} = 3.2 \times 10^{-6}$ s^{-1}.

III.3. Plasmon Band. In Figure 12, it is shown the plasmon band and a typical fitting through Lorentzians,[29] at two different times, for an electrolysis carried out at $j = -5$ mA cm^{-2} (similar results can be obtained for other current densities). It can be seen that the band is composed of two bands at short times and three bands at the later stages of the electrolysis.

The broad band located at $\lambda \geq 450$ nm, which does not appear at short times, can be attributed to the aggregation of particles in the synthesis medium. Its contribution can be eliminated just by centrifugation of the samples.

The most important contribution comes from the plasmon band, which was found to be located in the wavelength range $\lambda_P = 420-444$ nm, depending on the current density.[1] In our case, the plasmon band is red shifted with respect to its position reported by other authors. For example, Henglein and Mulvany

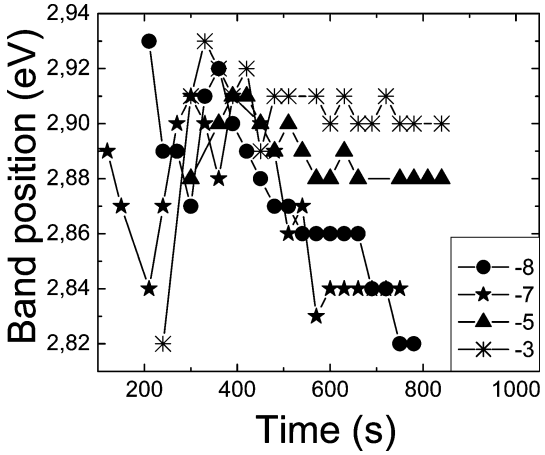

Figure 13. Change of the plasmon band position during the electrolysis at different current densities.

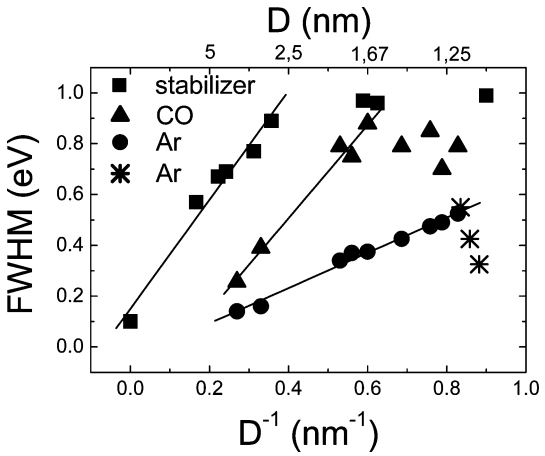

Figure 14. The fwhm versus particle size (D): stabilizer (our results), CO,[35] Ar,[42] Ar*.[43]

reported $\lambda_P = 380$ nm,[30,31] and Wiegel and Pohl found $\lambda_P = 405$ nm;[32,33] but it is known that the position of the plasmon band is very sensitive to changes in the particle surface.[34] Different facts can be responsible for the red shift observed: the high concentration of Ag^+ which is present in the solution and that probably charges the particles positively,[35,36] the presence of the stabilizer chain,[37−41] and the higher refraction index of the used solvent ($n_D^{20} = 1.3330$ from water versus $n_D^{20} = 1.3441$ from acetonitrile).

In Figure 13, one can see the change of the plasmon band position during the electrolysis, for different current densities. Besides the beginning, in which the estimation of the plasmon band position is doubtful, it can be observed a red shift of the plasmon band with both increasing time and current density. This can be correlated with the increase in the Ag^+ concentration (1.3×10^{-4}, 7.7×10^{-4}, 2×10^{-3}, 2.4×10^{-3} M; for $j = -1$ to $j = -7$ mA cm^{-2}, respectively[17]) and confirms the influence of the [Ag^+] on the observed plasmon band red-shift.

In our previous work we have shown that, according to different theories, the full width at half-maximum (fwhm) of the plasmon band increases linearly with the inverse of the particle size ($1/R$ law[44]). In Figure 14, it is shown the present results spanning now a large size range. It can be clearly seen that, although for the biggest particles the predicted linear relationship is fulfilled, the fwhm seems to attain a plateau for the smallest particles. This break of the $1/R$ law has been observed before,[45−47] and in the same figure we have plotted previous results of Ag particles deposited in different substrates

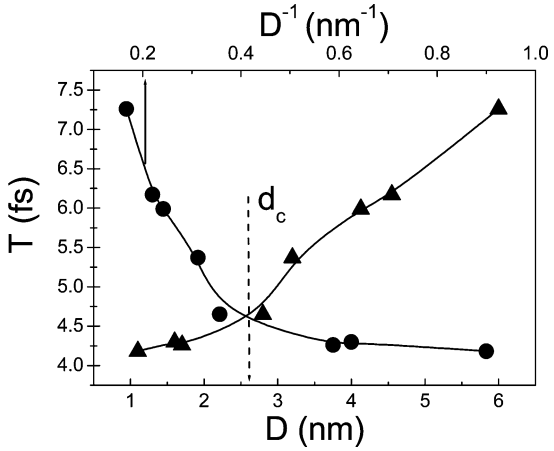

Figure 15. Plasmon relaxation time against particle size.

(CO and Ar), which have been used to interpret the influence of the matrix on the plasmon bandwidth. It can be clearly seen that the substrate influences the position of the $1/R$ break point. For Ar it appears at ≈1.2 nm; for CO it appears at ≈1.6 nm, and for the TBAAcO it appears at ≈2.5 nm. The existence of this break point can be related to the existence of different plasmon relaxation processes. In fact, it is known that the plasmon relaxation can be described as a sum of two processes:[48]

$$\text{fwhm} = \frac{h}{\tau}; \quad \frac{1}{\tau} = \frac{1}{\tau_{\text{R}}} + \frac{1}{\tau_{\text{NR}}} \tag{8}$$

where h is Planck's constant, τ_{R} and τ_{NR} are the radiative and nonradiative relaxation times, respectively, and τ is the global relaxation time.

In Figure 15, the plasmon relaxation time is represented against the particle size. It can be seen that the evolution of the relaxation time changes at $D \approx 2.5$ nm and seems to converge to a value of $\tau \approx 4$ fs for the smallest particles sizes. This value compares well with other previously reported values which are in the range 2−4 fs.[13] In these ranges of very small sizes ($D \leq$ 2.5 nm), the plasmon then predominantly relaxes with the formation of electron−hole (e−h) pairs instead of reemitting the photon.[49] It seems that this deactivation channel of the plasmon band creating an e−h is almost independent of the particle size. According to Figure 14, the relaxation via electron−holes is favored by the presence of TBAAcO as a stabilizing agent (comparing with other less interacting or noninteracting media), and this has been referred to, sometimes, as chemical relaxation[50] because it is assumed that the relaxation can be favored by the presence of chemical bonds at the particle surface.

Now we come to the third band which appears overlapping the plasmon band (see Figure 12). This ubiquitous band (which we will call, for the reasons given below, SE band), appearing at any of the employed current densities, is always observed as a shoulder of the plasmon band, and it is located at $\lambda_{\text{SE}} \cong 340$ nm. In a previous work, we have related this band to the presence of a long-living cluster. However, before a nonambiguous assignment of this band can be made, there are some experimental facts which have to be taken into account: (i) The band appears at approximately the same time as the appearance of the plasmon band and becomes more important with the increase in the current density, that is, when the particles produced in the reaction medium are very small (<2.5 nm). (ii) It shows, contrary to the plasmon band, a blue shift with both time and current density (this different behavior rules out the possibility that the band could be related with a possible splitting of the plasmon band as a result of a nonspherical shape of the particles, an aspect which has been in addition confirmed by TEM). (iii) The fwhm for the SE band also follows a $1/R$ law with approximately the same slope (19 ± 1 eV Å) as the fwhm of the plasmon band (21 ± 2 eV Å). It is difficult to understand all these facts just by assuming the band is due to a long-lived cluster. Another more plausible explanation is that the band could be related with a single electronic (SE) transition. As we have seen before, for the smallest particles ($D \leq$ 2.5 nm), plasmon deactivation takes place mainly through nonradiative channels (electron−hole pair formation); that is, the oscillating electrons lose their energy through the activation of single electronic transitions (Landau damping) with a relaxation time of the order of 4 fs, independently of the particle size. The deactivation process of the plasmon-activated electron−hole pair could then be related to the fwhm of the SE band and, more properly, to the faster electron−electron (e−e) scattering (e−e: 10−500 fs). However, more studies have to be done in order to check the true nature of this band.

IV. Discussion

Although the main discussion was already performed inside the different sections, we will include here some general discussions concerning the mechanism of particle formation and the properties of the plasmon band.

It has been said before that the observed change in the particle size with the current density has been explained in the past in thermodynamical terms: particles below a critical nucleus are energetically unstable because the driving force (in our case, the overpotential) to bring the atoms into a new phase (the solid particles) does not compensate the big Laplace force which occurs at low radius (high curvatures). However, this explanation does not take into account the well-known phenomenon that clusters of particular sizes ("magic numbers") are specially stabilized when the corresponding electronic shells are completed.[51,52] The number of atoms of the most stable clusters can be calculated for particles in a vacuum or in the gas phase by simple models, such as the jellium model,[53] but it is extremely difficult to make predictions for clusters in solution, especially if they are stabilized by particular capping molecules like those we have used in our study (TBAAcO). In any case, the observation of stable clusters in solution has been reported many times, and we have used this information to identify the clusters which are most probably present in our system, and in particular, the Ag_4^{2+} cluster. The identification of this cluster as a precursor of the obtained particles automatically rules out the previous thermodynamical argument. It remains, however, to explain why the particle size changes with the current density, but this is not a general result as it was believed before,[12] and indeed, we have also observed, in the electrochemical synthesis of Co particles, that the current density can increase, decrease, or even have no effect at all on the final particle size, depending on the used TBA counterion.[16] More studies have to be performed to clarify this aspect in which the adsorption of species onto the electrode where the particles are being formed (reduced) may play an important role.[54]

Concerning the observed break of the $1/R$ law for the plasmon band, one can see in Figure 14 that the presence of a chemical bond between Ag particles and TBAAcO induces a faster deactivation of the plasmon band. This can be deduced because the break is observed at high energies, that is, smaller relaxation times (see eq 8). For the smallest particles the corresponding

relaxation times for the plasmon decay are 4 fs (TBAAcO), 4.8 fs (CO), and 6.5 fs (Ar). One can also see that the break is observed for bigger particles when TBAAcO is present: 2.5 nm (TBAAcO), 1.7 nm (CO), and 1.2 nm (Ar). Therefore, one can say that, as the interactions increase (Ar < CO < TBAAcO), the oscillating electrons lose their energy to produce an electron−hole pair more easily. Wether this is related with a reduction of the electron density (remember that we have a big red shift of the plasmon band) or with an increase of the overlapping of the plasmon and SE bands[43] (there is an increase of the bandwidth with the reduction in size which may overcompensate the increase of the distance between the band peaks) is a matter which remains to be explored.

V. Conclusions

Through a time-resolved study of the absorption properties of Ag particles generated by the electrochemical technique we have studied the kinetics of the particle formation in the presence of TBAAcO as stabilizing agent. It has been observed that the particle formation takes place through the formation of several clusters, the Ag_4^{2+} being the most stable one. Analyzing the evolution of the Ag_4^{2+} band (λ_{250}) and the plasmon band (λ_P) with time, for experiments taken at different current densities, we were able to derive a mechanism of the particle formation. At the latest stages of the particle formation, one has to consider the electrodeposition which takes place in parallel to the formation of the particles, the influence of the electrodeposition being more important at low current densities. A value of the kinetic constant corresponding to the slow step of the mechanism, namely, the reduction of the more stable cluster, Ag_4^{2+}, has been deduced ($k_{4,1} = 3.2 \times 10^{-6}$ s^{-1}). From the fittings, the ratio of extinction coefficients $\epsilon_P/\epsilon_{250} = 0.7$ has been derived. If one takes into account previous data for the plasmon band extinction coefficient,[55] $\epsilon_P = 7200$ M^{-1} cm^{-1}, then an estimation of the extinction coefficient for the Ag_4^{2+} cluster can be made: $\epsilon_{250} = 1.0 \times 10^4$ M^{-1} cm^{-1}. This value agrees very well with previous reported values for the extinction coefficient of this cluster in water,[56,57] which is in the range $(1-4) \times 10^4$ M^{-1} cm^{-1}, and can be taken as independent proof of the proposed mechanism.

By analysis of the plasmon band, it has been observed that the $1/R$ relationship breaks down for particle sizes <2.5 nm, which could be related with a nonradiative plasmon dephasing due to the excitation of single-electron (SE) transitions. This transition could be related to the band (SE band) which always appears as a shoulder of the plasmon band and has an absorption maximum centered at ≈340 nm. The observed damping of the plasmon band to produce an electron−hole pair occurs more easily (i.e., smaller relaxation times) for the particles protected with TBAAcO obtained here than for isolated particles (in an Ar matrix) or for particles slightly interacting with the surrounding medium (in a CO matrix). Because the field enhancement at the particle surface is proportional to the relaxation time of the plasmon, it seems that strong interactions diminish the field enhancement. This can have important consequences in different fields, such as plasma-assisted optical guides,[58] SERS,[59] near-field optical phenomena,[60] and the conversion of plasmons into quasi-particles[61] (e−h pairs), which is a very interesting topic which can have important consequences in nanotechnological applications in the near future.

Acknowledgment. We thank the financial support of the Spanish Ministry of Science and Technology (Project No. MAT2002-00824). M.L.R.S. also thanks a grant from the Consellería de Educación of the Xunta de Galicia.

References and Notes

(1) Králik, M.; Biffis, A. *J. Mol. Catal. A: Chem.* **2001**, *177*, 113.
(2) Schatz, G. C. Electromagnetic Mechanism of Surface-Enhanced Spectroscopy. In *Handbook of Vibrational Spectroscopy*; Chalmers, J. M., Griffiths, P. R., Eds.; John Wiley & Sons: Chichester, U.K., 2002; pp 1−16.
(3) Sellmyer, D. J.; Yu, M.; Kirby, R. D. *Nanostruct. Mater.* **1999**, *12*, 1021.
(4) Shipway, A. N.; Katz, E.; Willner, I. *ChemPhysChem* **2000**, *1*, 18.
(5) López-Quintela, M. A. *Curr. Opin. Colloid Interface Sci.* **2003**, *8*, 137.
(6) Manna, A.; Imae, T.; Iida, M.; Hisamatsu, N. *Langmuir* **2001**, *17*, 6000.
(7) Kiwi, J.; Grätzel, M. *J. Am. Chem. Soc.* **1979**, *101*, 7214.
(8) Reetz, M. T.; Helbig, W. *J. Am. Chem. Soc.* **1994**, *116*, 7401.
(9) Zova, J. V.; Stieger, R. M.; Biernacki, P. R.; Penner, R. M. *J. Phys. Chem.* **1996**, *100*, 837.
(10) Hodes, G., Ed. *Electrochemistry of Nanomaterials*; Wiley-VCH: Weinheim, Germany, 2001.
(11) Rodríguez-Sánchez, L.; López-Quintela, M. A.; Blanco, M. C. *J. Phys. Chem. B* **2000**, *104*, 9683.
(12) Pascal, C.; Pascal, J. L.; Favier, F.; Elidrissi Moubtassim, M. L.; Payen, C. *Chem. Mater.* **1999**, *11*, 141.
(13) Chang, S.-S.; Shih, C.-W.; Chen, C.-D.; Lai, W.-C.; Wang, C. R. C. *Langmuir* **1999**, *15*, 701.
(14) Reetz, M. T.; Winter, M.; Breinbauer, R.; Thurn-Albrecht, T.; Vogel, W. *Chem.−Eur. J.* **2001**, *7*, 1084.
(15) Maier, S. A.; Kik, P. G.; Atwater, H. A.; Meltzer, S.; Requicha, A. A. G.; Koel, B. E. *Proc. SPIE−Int. Soc. Opt. Eng.* **2003**, *4810*.
(16) Sandell, E. B. *Colorimetric Metal Analysis*; Interscience Publishers: New York, 1959.
(17) Rodríguez-Sánchez, L. Ph.D. Thesis, University of Santiago de Compostela, Spain, 2003.
(18) Henglein, A.; Schnabel, W.; Wendenburg, J. *Einführung in die Strahlenchemie*; Verlag Chemie: Weinheim, Germany, 1969.
(19) Henglein, A. *Chem. Phys. Lett.* **1989**, *154*, 473.
(20) Henglein, A.; Linnert, T.; Mulvaney, P. *Ber. Bunsen-Ges. Phys. Chem.* **1990**, *94*, 1449.
(21) Tausch-Treml, R.; Henglein, A.; Lilie, J. *Ber. Bunsen-Ges. Phys. Chem.* **1978**, *82*, 1335.
(22) Ershov, B. G.; Janata, E.; Henglein, A.; Fojtik, A. *J. Phys. Chem.* **1993**, *97*, 4589.
(23) Linnert, T.; Mulvaney, P.; Henglein, A. *J. Phys. Chem.* **1991**, *97*, 679.
(24) Mulvaney, P.; Henglein, A. *J. Phys. Chem.* **1990**, *94*, 4182.
(25) Zheng, J.; Dickson, R. M. *J. Am. Chem. Soc.* **2002**, *124*, 13982.
(26) Maali, A.; Cardinal, T.; Treguer-Delapierre, M. *Physica E* **2003**, *17*, 559.
(27) Felix, C.; Sieber, C.; Harbich, W.; Buttet, J.; Rabin, I.; Schulze, W.; Ertl, G. *Phys. Rev. Lett.* **2001**, *86*, 2992.
(28) Peyser, L. A.; Vinson, A. E.; Bartko, A. P.; Dickson, R. M. *Science* **2001**, *291*, 103.
(29) Kittel, C. *Introduction to Solid State Physics*, 2nd ed.; Wiley: New York, 1956.
(30) Henglein, A. *J. Phys. Chem.* **1993**, *97*, 5457.
(31) Mulvaney, P. *Langmuir* **1996**, *12*, 788.
(32) Wiegel, E. *Z. Phys.* **1954**, *136*, 642.
(33) Pohl, R. W. *Einführung in die Optik*, 7th and 8th eds.; Springer-Verlag: Berlin, Germany, 1948; pp 209.
(34) See, for example, the following: Lyon L. A.; Peña, D. J.; Natan, M. J. *J. Phys. Chem. B* **1999**, *103*, 5826.
(35) Henglein, A. *J. Phys. Chem.* **1979**, *83*, 2209, 2858.
(36) Henglein, A. *Ber. Bunsen-Ges. Phys. Chem.* **1980**, *84*, 253.
(37) Underwood, S.; Mulvaney, P. *Langmuuir* **1994**, *10*, 3427.
(38) Wilcoxon, J. P.; Williamson, R. L.; Baughman, R. J. *J. Chem. Phys.* **1993**, *98*, 993.
(39) Torgoe, K.; Nakajima, Y.; Esumi, K. *J. Phys. Chem.* **1993**, *97*, 8304.
(40) Esumi, K.; Shiratori, M.; Ishizuka, H.; Tano, T.; Torigoe, K.; Meguro, K. *Langmuir* **1991**, *7*, 457.
(41) Malinsky, M. D.; Kelly, K. L.; Schatz, G. C.; Van Duyne, R. P. *J. Am. Chem. Soc.* **2001**, *123*, 1471.
(42) Charlé, K. P.; König, L.; Rabin, I.; Schulze, W. *Z. Phys. D: At., Mol. Clusters* **1996**, *36*, 159.
(43) Harbich, W.; Fedrigo, S.; Buttet, J. *Z. Phys. D: At., Mol. Clusters* **1993**, *26*, 138.
(44) Kreibig, U.; Fragstein, C. V. *Z. Phys.* **1969**, *224*, 307.
(45) Fragstein, C. V.; Römer, H. *Z. Phys.* **1958**, *151*, 54.
(46) Doyle, W. T. *Phys. Rev.* **1958**, *111*, 1067.
(47) Hampe, W. *Z. Phys.* **1958**, *152*, 470.

(48) Heilweil, E. J.; Hochstrasser, R. M. *J. Chem. Phys*. **1985**, *82*, 4762−4770.
(49) Molina, R. A.; Weinmann, D.; Jalabert, R. A. *Phys. Rev. B: Solid State* **2002**, *65*, 155427.
(50) Kreibig, U.; Vollmer, M. *Optical Properties of Metal Clusters*; Springer-Verlag: Berlin, Germany, 1995.
(51) Knigth, W. D.; Clemenger, K.; de Heer, W. A.; Saunders, W. A.; Chou, M. Y.; Cohen, M. L. *Phys. Rev. Lett*. **1984**, *52*, 2141.
(52) Gölich, H.; Lange, T.; Bergmann, T.; Martin, T. P. *Phys. Rev. Lett*. **1990**, *65*, 748.
(53) Eckardt, W. *Phys. Rev. B: Solid State* **1984**, *29*, 1558.
(54) Cao, P.; Sun, Y.; Gu, R. *J. Phys. Chem. B* **2003**, *107*, 5818.
(55) Petit, C.; Lixon, P.; Pileni, M.-P. *J. Phys. Chem*. **1993**, *97*, 12974.
(56) Ershov, B. G.; Janata, E.; Henglein, A.; Fojtik, A. *J. Phys. Chem*. **1993**, *97*, 4589.
(57) Henglein, A.; Trausch-Treml, R. *J. Colloid Interface Sci*. **1981**, *80*, 84.
(58) Maier, S. A.; Kik, P. G.; Atwater, H. A.; Meltzer, S.; Harel, E.; Koel, B. E.; Requicha, A. A. G. *Nat. Mater*. **2003**, *2*, 229.
(59) Michaels, A. M.; Nirmal, M.; Brus, L. E. *J. Am. Chem. Soc*. **1999**, *121*, 9932.
(60) Krenn, J. R.; Dereux, A.; Weeber, J. C.; Bourillot, E.; Lacroute, Y.; Goudonnet, J. P.; Shider, G.; Gotshy, W.; Leitner, A.; Aussenegg, F. R.; Girard, C. *Phys. Rev. Lett*. **1999**, *82*, 2590.
(61) Klar, T.; Perner, M.; Grosse, S.; von Plessen, G.; Spirkl, W.; Feldman, J. *Phys. Rev. Lett*. **1998**, *80*, 4249.